Molecular Cancer Therapeutics

Dimethyl Fumarate Controls the NRF2/DJ-1 Axis in Cancer Cells: Therapeutic Applications

Nathaniel Edward Bennett Saidu[1], Gaëlle Noé[2], Olivier Cerles[1], Luc Cabel[1], Niloufar Kavian-Tessler[1], Sandrine Chouzenoux[1], Mathilde Bahuaud[1], Christiane Chéreau[1], Carole Nicco[1], Karen Leroy[1,3], Bruno Borghese[4], François Goldwasser[1,5], Frédéric Batteux[1,6], and Jérôme Alexandre[1,5]

Abstract

The transcription factor NRF2 (NFE2L2), regulates important antioxidant and cytoprotective genes. It enhances cancer cell proliferation and promotes chemoresistance in several cancers. Dimethyl fumarate (DMF) is known to promote NRF2 activity in noncancer models. We combined *in vitro* and *in vivo* methods to examine the effect of DMF on cancer cell death and the activation of the NRF2 antioxidant pathway. We demonstrated that at lower concentrations (<25 μmol/L), DMF has a cytoprotective role through activation of the NRF2 antioxidant pathway. At higher concentrations, however (>25 μmol/L), DMF caused oxidative stress and subsequently cytotoxicity in several cancer cell lines. High DMF concentration decreases nuclear translocation of NRF2 and production of its downstream targets. The pro-oxidative and cytotoxic effects of high concentration of DMF were abrogated by overexpression of NRF2 in OVCAR3 cells, suggesting that DMF cytotoxicity is dependent of NRF2 depletion. High concentrations of DMF decreased the expression of DJ-1, a NRF2 protein stabilizer. Using DJ-1 siRNA and expression vector, we observed that the expression level of DJ-1 controls NRF2 activation, antioxidant defenses, and cell death in OVCAR3 cells. Finally, antitumoral effect of daily DMF (20 mg/kg) was also observed in *vivo* in two mice models of colon cancer. Taken together, these findings implicate the effect of DJ-1 on NRF2 in cancer development and identify DMF as a dose-dependent modulator of both NRF2 and DJ-1, which may be useful in exploiting the therapeutic potential of these endogenous antioxidants. *Mol Cancer Ther; 16(3); 529–39. ©2017 AACR.*

Introduction

Dimethyl fumarate (DMF) is a derivative of fumaric acid registered for the treatment of relapsing forms of multiple sclerosis and psoriasis (http://www.fda.gov; refs. 1–3). Several studies have shown its cytoprotective and antioxidant effects in noncancer models (1–5), which appeared related to the induction of the nuclear factor erythroid 2 (NF-E2)-related factor 2 (NRF2) pathway (2–6). NRF2 is a ubiquitously expressed basic leucine zipper transcription factor (7–9). It is a "Master redox switch" as it is known to induce cytoprotective genes that render protection of cells from oxidative stress (OS; refs. 10, 11). At physiologic levels, NRF2 is held in the cytoplasm as an inactive complex bound to Kelch-like ECH-associated protein 1 (KEAP1), a repressor molecule that facilitates NRF2 ubiquitination. By inducing covalent modification of thiols in some of the cysteine residues of KEAP1, DMF leads to conformational changes in KEAP1 that ultimately result in disruption of the KEAP1–NRF2 interaction, thereby, warranting the translocation of NRF2 into the nucleus. Within the nucleus, NRF2 binds to the antioxidant response element (ARE) in the promoter region of phase II genes and stimulates their transcription (10, 11).

On the other hand, the cytotoxic effect of DMF against several tumor cell lines has been suggested *in vitro* (12–16) and the induction of oxidative stress has also been reported (17, 18). These observations however, are somehow conflicting with the role of NRF2 in cancer cells. NRF2 accumulation was detected in many cancers, where it has been proven to act as an oncogene (7, 9). It could limit to an acceptable level the accumulation of reactive oxygen species produced in excess by the mitochondrial respiratory chain in hypermetabolic and proliferative cancer cells. Overexpression of the NRF2 protein has also recently emerged as a potential mechanism of resistance to platinum and other cytotoxicities (7–9).

DMF may have other molecular targets, such as DJ-1. DJ-1 is a multifunctional protein that is encoded by the *PARK7* gene. It has antioxidant properties and it regulates NRF2-dependent antioxidant signaling by preventing its association with KEAP1 thereby promoting its stability and activation (19, 20).

In this report, we demonstrated that DMF has a dose-dependent effect in cancer cells, cytoprotective at lower concentrations by inducing NRF2; it inhibits at higher concentrations the NRF2 stabilizer DJ-1, which in turn inhibits NRF2 activation, induces OS, and subsequently promotes cancer cell death. These findings

[1]Paris Descartes University, Sorbonne Paris Cité, INSERM U1016, Cochin Institute, CARPEM, Paris, France. [2]UMR8638 CNRS, Faculté de Pharmacie, Université Paris Descartes, PRES Sorbonne Paris Cité, Paris, France. [3]Department of Molecular Genetics, Cochin Hospital, AP-HP, Paris, France. [4]Department of Gynecologic Surgery, Cochin Hospital, AP-HP, Paris, France. [5]Department of Medical Oncology, Cochin Hospital, AP-HP, Paris, France. [6]Department of Immunology, Cochin Hospital, AP-HP, Paris, France.

Note: Supplementary data for this article are available at Molecular Cancer Therapeutics Online (http://mct.aacrjournals.org/).

Corresponding Author: Jérôme Alexandre, Cochin Hospital, AP-HP, Paris Descartes University, 123 boulevard de Port Royal, Paris 75014, France. Phone: 331-5841-1927; Fax: 331-5841-1929; E-mail: jerome.alexandre@aphp.fr

doi: 10.1158/1535-7163.MCT-16-0405

implicate the effect of DJ-1 on NRF2 in cancer development and identify DMF as not only an activator, but also an inhibitor of both NRF2 and DJ-1, which may be useful in exploiting the therapeutic potential of these endogenous antioxidants.

Materials and Methods

Reagents and antibodies

Protease inhibitor cocktail Complete was obtained from Roche Diagnostics, and paclitaxel was obtained from Fresenius Kabi. Brusatol was from Carbosynth. The Nucleobond AX-plasmid-purification kit was from Macherey-Nagel, NIH:OVCAR-3 Cell Avalanche Transfection Reagent was from EZ Biosystems. pGW1-Myc-DJ-1-WT and pCDNA3.1FLAGNRF2 were from Addgene (plasmids, #29347 and #36971). DJ-1 siRNA kit, antibodies against NRF2, DJ-1, β-actin, and GAPDH were all purchased from Santa Cruz Biotechnology. Anti-PARP, anti-caspase-3, anti-Myc, anti-Lamin A, and anti-Flag were purchased form Cell Signaling Technology. Goat, mouse, and rabbit secondary antibodies were all bought from Dianova. All other chemicals (except when and where stated) were from Sigma.

Cell culture

OVCAR3 (human serous ovarian carcinoma), TOV 21G (human clear ovarian carcinoma), CT26 (mouse colon carcinoma), HT29 (human colon carcinoma), SW40 (human colon carcinoma), Caco-2 (human colon carcinoma), A549 (human lung adenocarcinoma), MCF7 (human breast carcinoma), and Mia Paca-2 (human pancreatic carcinoma) were all obtained from the ATCC in April 2012, where cell lines were authenticated by short tandem repeat profiling. These cells were not reauthenticated by our laboratory but stocks were instead kept frozen until initiation of these studies. OVCAR3 and TOV 21G cells were cultured in RPMI1640 containing insulin (10 μg/mL). MCF7 cells were cultured in DMEM/F-12, whereas HT29 and SW480 cells were cultured in McCoy 5A. All other cells were cultured in DMEM/Glutamax-I. The primary human lung cancer cell line was a gift from Prof. D Damotte and Prof. M Alifano (Departments of Pathology and Thoracic Surgery, Cochin Hospital, Paris, France) and its use was authorized by the patient. All the culture media were supplemented with 10% heat-inactivated FBS and antibiotics (Life Technologies). Cells were cultured in an atmosphere enriched with 5% CO_2. They were passaged every 3 days and routinely tested to rule out mycoplasma infection. The seeding of cells, time of treatment, and concentration of agents are shown in the figures and/or corresponding figure legends.

Animal studies

BALB/cJRj female mice between 6 and 8 weeks of age were used in all experiments (Iffa Credo). Animals received humane care in compliance with the institutional guidelines. Two set of studies were done to evaluate the effect of DMF in *vivo*: (1) preventive (21) effect of DMF in a chemically induced colon cancer mouse model and (2) antitumoral effect of DMF in mice bearing CT26-implanted tumors. The daily dose of 20 mg/kg DMF that is associated with antitumoral effect was used on the basis of previously published data (12, 13).

For model (1), we followed a published protocol (21–23) to induce colon cancers using two drugs: azoxymethane (AOM) that causes O6-methylguanine formation and dextran sulfate sodium salt (DSS) that induces chronic inflammation. Twenty-two BALB/cJRj mice were divided into two experimental groups (groups 1 and 2, 9 mice each) and 1 control group (group 3, no AOM/DSS, 4 mice). Groups 1 and 2 were given a single intraperitoneal injection (i.p.) of AOM (10 mg/kg body weight). Starting day 7 after the injection, groups 1 and 2 received 2% DSS in drinking water for 7 days. On day 14, cages were switched back to standard drinking water for 3 weeks. A cycle consisting of 1 week of DSS in drinking water followed by 3 weeks of standard drinking water was carried out for two additional times. Starting day 7 after the AOM injection, mice were fed by gauge daily with DMSO and 20 mg/kg DMF to groups 1 and 2, respectively. In addition, control mice received no AOM/DSS and were fed the normal pelleted diet with regular drinking water. At the end of week 20, blood samples were retro-orbitally punctioned from all the animals for advanced oxidized protein products (AOPP) analysis before anesthetizing and sacrificing them. The colons were flushed with PBS and excised. Their length was measured (from the ileocecal junction to the anal verge), and they were cut open longitudinally along the main axis before washing with PBS. As previously described, the incidence of rectal prolapses and the shortened length of colons were indicative of colorectal cancer formation (24). The number of visible (by eye) tumors (appearance of intestinal mucosa, nodular, polypoid, or caterpillar-like) was counted.

2) CT26 tumor cells were resuspended in Gibco GlutaMAX media and injected subcutaneously (1.5×10^5 cells/mouse) into the back of BALB/cJRj mice. When tumors reached a mean size of 200–500 mm^3 (day 0), animals were randomized, and put into four groups of 6 each. Animals in group 1 were treated daily by gauge with DMSO, groups 2 and 3 were each treated by intraperitoneal injections with 20 mg/kg paclitaxel for 3 days (day 0, 2, and 4). In addition, group 3, along with group 4 was treated daily by gauge with 20 mg/kg DMF. Tumor size was measured with a numeric caliper every 3 days. Tumor volume was calculated as follows: TV (mm^3) = $(L \times W^2)/2$, where L is the longest and W is the shortest radius of the tumor in millimeters. Results were expressed as means ± SD of tumor volumes ($n = 6$ in each group).

Histologic and immunohistochemical analysis

For histopathologic evaluation, colon samples were fixed in 4% formaldehyde and paraffin embedded. Sections (5 μm) were stained with hematoxylin and eosin before examining under a Nikon Eclipse 80i microscope with a Nikon PlanFluor 10× objective. Expression of NRF2 in mice tumors was evaluated by IHC as described previously (25). Briefly, tumors were excised and fixed in 4% formaldehyde and paraffin embedded. Sections (5 μm) were cut and labeled with anti-NRF2 antibody (1:500, Santa Cruz Biotechnology, sc-722) and DAB staining. Images were collected using a Nikon Eclipse 80i microscope with a Nikon PlanFluor 40× objective. As NRF2 staining was patchy throughout the samples, tumors were scored as either positive or negative for NRF2. For the quantification of nuclear NRF2, 50 nuclei were selected from NRF2-positive staining sections in tumors ($n = 6$ by treatment group). In each selected area, the number of NRF2-positive nuclei was counted among 50 nuclei and in each treatment group and from this, localized nuclear NRF2 was counted and expressed as a percentage relative to DMSO-treated group.

Transient transfection

Transfection of cells with plasmids was performed by using the NIH:OVCAR-3 Cell Avalanche Transfection Reagent according to the manufacturer's instructions. Briefly, OVCAR3 cells were

seeded into either a 60-mm dish (1×10^5 cells) in a total volume of 2.5 mL of cell culture medium or in a 96-well plate (0.5×10^4 cells) in a total volume of 100 μL of cell culture. Cells were cultured overnight and were then transfected with the NIH: OVCAR-3 Cell Avalanche Transfection Reagent using a total of 0.1 μg (96-well plate) or 0.25 μg (6-well plate) of plasmid DNA. DJ-1 siRNA transfections were also done according to the manufacturer's instructions. After 24 hours of cultivation, the medium was replaced by a fresh one; the cells were cultured for an additional 12–18 hours before treatment and then harvested for Western blot analysis.

Evaluation of cell viability and cell death

Cancer cells lines were seeded at 0.5×10^4 cells per well to a final volume of 100 μL in a 96-well plate and incubated overnight. Cells were then treated with DMSO (solvent control), different concentrations of DMF, or left untreated as indicated in figures and/or corresponding figure legends. The number of adherent cells was determined by a crystal violet assay as described previously (26). Results are expressed as a percentage of either cell number ± SEM versus DMSO-treated cells or cell number ± SEM versus cells in culture medium alone. Cell death was assessed by the expression of cleaved caspase-3 and PARP.

Intracellular ROS measurement

Cells were seeded at 1×10^4 cells per well to a final volume of 100 μL in a 96-well plate and incubated overnight. Cells were then treated with DMSO (solvent control), test compounds, or left untreated for different time periods as indicated in the figures. ROS was then assessed spectrofluorimetrically by oxidation of 2′,7′-di-chlorodihydrofluorescein diacetate (H_2DCFDA) as described previously (26). Fluorescence intensity was recorded every 1 hour for 6 hours at excitation and emission wavelengths of 485 and 530 nm, respectively. The number of cells was evaluated by the crystal violet assay and the level of ROS in each sample was calculated as follows: ROS levels (arbitrary units min^{-1} 10^4 $cells^{-1}$) = [Fluorescence intensity (arbitrary units) at T360 min – Fluorescence intensity (arbitrary units) at T0 min] per 60 minutes per number of cells as measured by the crystal violet assay. The final ROS figure (arbitrary units min^{-1} 10^4 $cells^{-1}$) was then expressed as a percentage relative to control.

Intracellular GSH measurement

Intracellular glutathione (GSH) levels were assessed as described previously (27). Briefly, cells seeded in 96-well plates were washed in PBS and incubated with 100 μL/well of 50 μmol/L monochlorobimane in PBS. To measure total oxidized GSH levels, free sulfhydryl groups were masked with 1.25% 2-vinylpyridine, dissolved in 125 mmol/L Na_2HPO_4 supplemented with EDTA 6.3 mmol/L (pH 7.5) for 1 hour and then processed as described previously (28). GSH levels were then assayed using a fusion spectrofluorimeter. Fluorescence intensity was recorded every 1 hour for 6 hours at excitation and emission wavelengths of 405 and 460 nm, respectively. The number of cells was evaluated by the crystal violet assay and the level of GSH in each sample was calculated as follows: GSH levels (arbitrary units min^{-1} 10^4 $cells^{-1}$) = [Fluorescence intensity (arbitrary units) at T360 min – Fluorescence intensity (arbitrary units) at T0 min] per 60 minutes per number of cells as measured by the crystal violet assay. The final total GSH figure (arbitrary units min^{-1} 10^4 $cells^{-1}$) was then expressed as a percentage relative to control.

Western blot analysis and immunoprecipitation

Extraction of total, nuclear, and cytosolic cellular proteins was performed as described previously (29, 30). The protein content of the supernatant was determined according to the Bradford method using the Bio-Rad protein assay reagent (Bio-Rad). SDS-PAGE and immunoblotting was also performed as described previously (29, 30). Briefly, proteins separated on a 7.5%, 10%, 12.5%, or 15% SDS-PAGE gel were transferred to a polyvinylidene difluoride (PVDF) membrane. Membrane was blocked with 5% dry milk in PBS containing 0.1% Tween-20 (PBST) for 1 hour at room temperature and then incubated with the specific primary antibody, which was diluted in PBST containing 1% dry milk powder. The membrane was washed with PBST (3× for 10 minutes), before being incubated with a peroxidase-coupled secondary antibody diluted in PBST for 1 hour at room temperature. The membrane was washed again in PBST (3× for 10 minutes). Signals were developed, visualized, and quantified using the FujiFilm LAS – 3000 imaging system. Immunoprecipitation (IP) was performed to detect the interaction between NRF2 and DJ-1. The immunoprecipitation procedures are provided in the Supplementary Data.

Statistical analysis

GraphPad Prism (GraphPad Inc.) software was used to analyze the data. All values are averages of at least three independent experiments made in triplicates, except when specified. Error bars shown in the figures represent SEM and all results were expressed as arithmetic mean ± SEM. Differences between the experimental groups were analyzed using one-way ANOVA or Student *t* test (two-tailed, unpaired), and statistically significant differences were shown as follows: **, $P < 0.01$; *, $P < 0.05$.

Results

High concentrations of DMF display cytotoxicity in several cancer cell lines and induce parallel increase of oxidative stress and GSH depletion

Previous studies have shown that at higher concentrations (50–200 μmol/L), DMF is capable of inhibiting melanoma and colon cancer cell growths (12, 13). In the current study, we therefore asked whether DMF treatment might have an influence on the viability of other cancer cell types. Hence, eight different human cancer cell lines, namely OVCAR3, TOV 21G, MiaPaca2, HT29, Caco-2, SW-480, MCF7, A549, and primary lung adenocarcinoma (P) along with one mouse CT26 cells were all treated with 100 μmol/L of DMF for 24, 48, and 72 hours. Cell viability was then evaluated by the crystal violet assay. As shown in Fig. 1A, DMF treatment resulted in loss of cell viability in a time-dependent manner in all the cell lines. The degree of cytotoxicity on the selected cell lines varied, and it was found to be most potent on Mia Paca-2 pancreatic carcinoma cells. In addition, the cleavage of caspase-3 (Fig. 1B, top) along with its substrate PARP (Fig. 1B, bottom), well-known events in the apoptotic process, were induced by high-dose DMF (100 μmol/L). Interestingly, lower concentrations of DMF (0.25–5 μmol/L) did not have any significant effect on cell viability (Supplementary Fig. S1A–S1D), caspase-3, or PARP cleavage (Supplementary Fig. S2A–S2D) in any of the selected cell lines.

As shown in Fig. 1C, treatment of cancer cells with 100 μmol/L DMF induced a time-dependent increase in ROS, in parallel to total GSH depletion (Fig. 1D), the body's master antioxidant. This

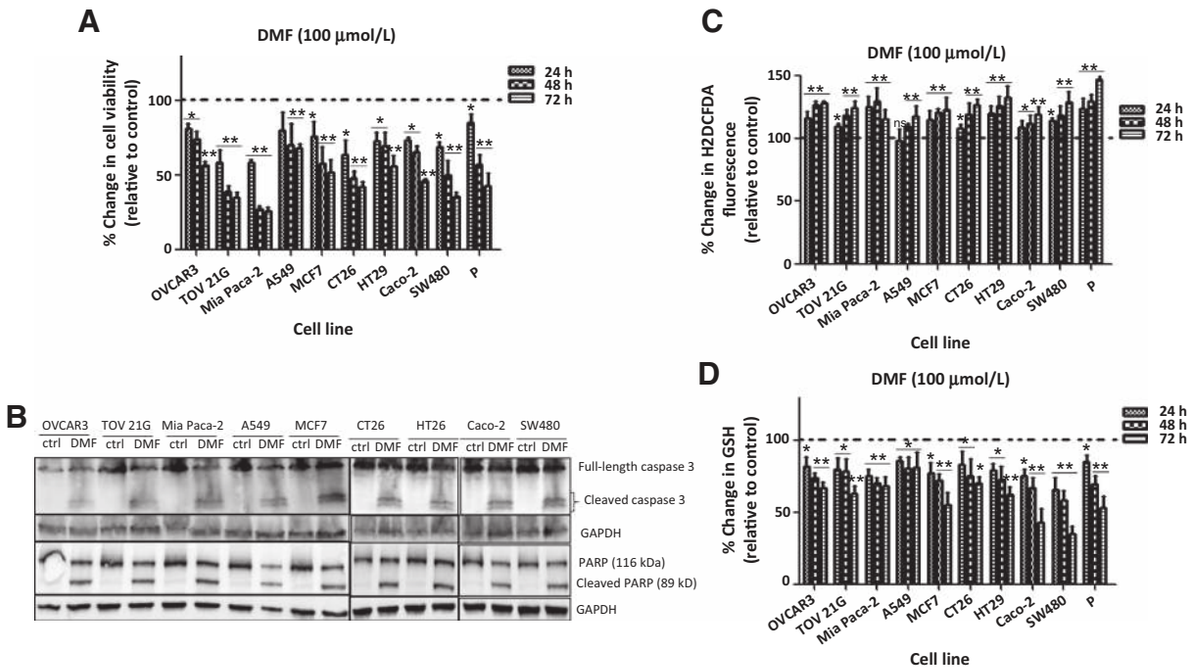

Figure 1.

Effect of DMF on cancer cells. **A,** Cancer cells were seeded in 96-well plates overnight and were treated with 0.05% DMSO (control = ctrl) or with 100 μmol/L DMF for 24, 48, and 72 hours. Cell viability was determined using the crystal violet assay method. Data are depicted as means ± SEM, ($n = 3$). **B,** Cells were treated with DMSO or 100 μmol/L DMF for 24 hours. Caspase-3 activation and cleavage of its downstream target PARP were analysed by Western blot analysis. GAPDH was used as a loading control. One representative of at least 3 Western blots is shown here. **C,** ROS produced in cancer cells following treatment with 100 μmol/L DMF for 24, 48, and 72 hours. **D,** Changes in total GSH levels measured in cancer cells 24, 48, and 72 hours after treatment with DMF. In all the experiments, data are expressed as a percentage change relative to control. In each case, the mean of three independent experiments is shown. *, $P < 0.05$; **, $P < 0.01$; ns, not statistically significant; P, primary cell line from a patient with lung adenocarcinoma.

DMF effect is also dose-dependent as treatment of OVCAR3 cells with different concentrations of DMF resulted in both a dose-dependent increase in ROS, in parallel to total GSH depletion (Supplementary Fig. S3A and S3B). Moreover, DMF caused a significant increase in oxidized GSH (GSSG) and a significant decrease in reduced GSH; both of which were concentration dependent (Supplementary Fig. S3C). Our results therefore suggest that DMF-induced ROS formation can lead to thiol oxidation and depletion in cancer cells. Next, we analyzed whether we could prevent DMF-induced cell death by pretreatment of cells with the GSH precursor *N*-acetyl cysteine (NAC). Indeed, NAC significantly prevented the DMF-induced oxidative stress (Supplementary Fig. S3D) and cytotoxicity at 24 hours (12.6%, $P < 0.05$) and even more so at 48 hours (27.3%, $P < 0.01$; Supplementary Fig. S3E). These data strongly suggest that cancer cell death induced by high concentration of DMF is related to oxidative stress.

Low concentrations of DMF induce NRF2 activation and are cytoprotective

As we observed no significant change in cell viability with lower concentrations of DMF (0.25–5 μmol/L), but a rather significant increase in GSH levels in OVCAR3 cells (Supplementary Fig. S3B and S3C), we hypothesized that low concentrations of DMF may be cytoprotective through activation of the NRF2 antioxidant pathway. To test this hypothesis, we first treated OVCAR3 cells with DMF alone or in combination with the NRF2 small-molecule inhibitor brusatol (Bru; ref. 31). OVCAR3 cells were chosen for all subsequent experiments because the cytotoxicity of DMF in this cell line appeared as the mean of all tumor cell lines and OVCAR3 cells were also more sensitive to paclitaxel, a drug we were also interested in testing. Furthermore, OVCAR3 cells express high levels of NRF2. As shown in Fig. 2A, 5 μmol/L DMF induced nuclear accumulation of NRF2 protein which was abrogated when cells were treated with brusatol in addition to DMF. To further showcase the cytoprotective capability of low-dose DMF, OVCAR3 cells were treated with DMSO (ctrl), paclitaxel, or brusatol, alone or in combination with 5 μmol/L DMF. As a positive control, we treated the cells with epigallocatechin-3-gallate (EGCG), which is known to induce ROS formation and cause cell death. Compared with DMSO control–treated cells, paclitaxel and brusatol significantly reduced cell viability. Peculiarly, 5 μmol/L DMF significantly reduced the cytotoxicity of paclitaxel (Fig. 2B). In parallel, DMF also significantly reduced paclitaxel-induced ROS, confirming the cytoprotective capability of low-dose DMF. In contrast, DMF was unable to prevent oxidative stress and cytotoxicity induced by brusatol (Fig. 2B and C). Thus, low concentrations of DMF display cytoprotective and antioxidant effects that appear related to NRF2 activation.

DMF cytotoxicity is dependent on NRF2 depletion

Given the cytotoxic effect of high concentrations of DMF, we wondered whether NRF2 expression and activity is dependent on DMF concentration. Indeed, we observed that total NRF2

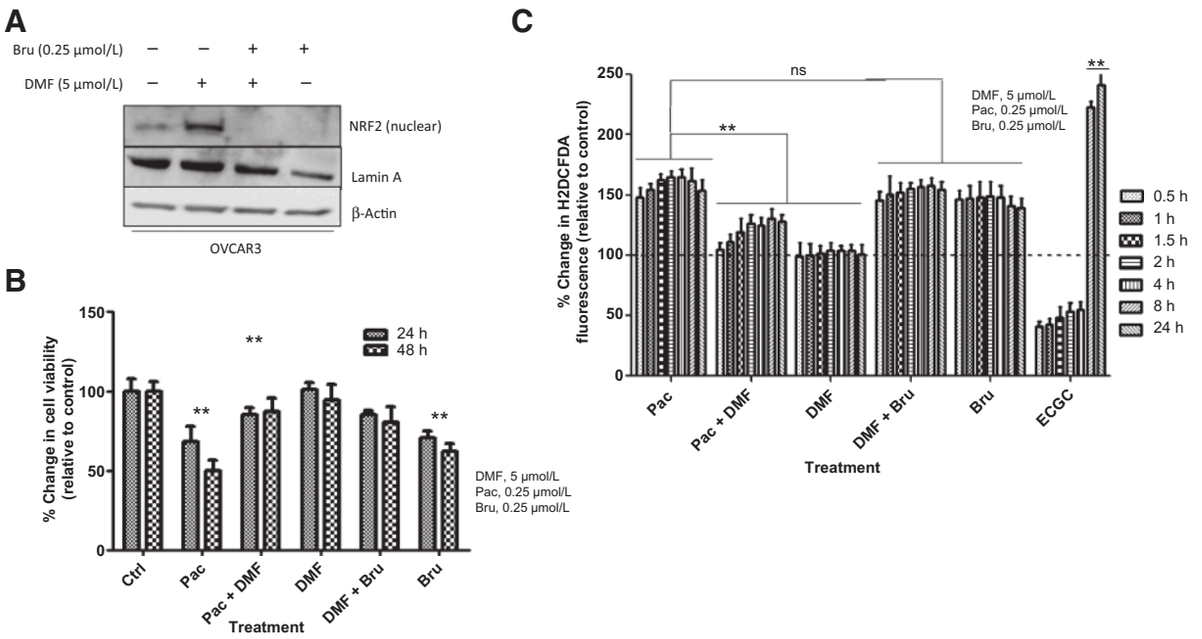

Figure 2.

Cytoprotective effects of low concentrations of DMF. **A,** OVCAR3 cells were treated with 5 μmol/L DMF alone, 5 μmol/L DMF in combination with 0.25 μmol/L brusatol (Bru), 0.25 μmol/L brusatol alone or cells left untreated for 24 hours. Nuclear and cytosolic protein lysates were prepared and analyzed on a 10% SDS-polyacrlamide gel followed by Western blottting using an anti-NRF2–specific antibody. Lamin A was used as a nuclear marker, while β-actin was used as a loading control. One representative of at least two Western blots is shown here. **B** and **C,** OVCAR3 cells were seeded in 96-well plates overnight and treated the following day with 0.05% DMSO (ctrl), 0.25 μmol/L paclitaxel (Pac), 5 μmol/L DMF, 0.25 μmol/L brusatol, 0.25 μmol/L paclitaxel (Pac) in combination with 5 μmol/L DMF or with 0.25 μmol/L brusatol in combination with 5 μmol/L DMF for the indicated times shown in the figure. Epigallocatechin-3-gallate (EGCG) was used as a positive control for ROS production. Cell viability (**B**) was determined using the crystal violet assay method. In all the experiments, data are expressed as a percentage change relative to control. In each case, the mean of three independent experiments is shown. *, $P < 0.05$; **, $P < 0.01$; ns, not statistically significant.

expression was increased by low concentration of DMF but at a decreasing level with subsequent increase in DMF concentration in OVCAR3 cells (Fig. 3A). Moreover, it was evident in OVCAR3 (Fig. 3B) and TOV 21G (Supplementary Fig. S4A) cells that only the nuclear, active, fraction of NRF2 was decreased by high concentration of DMF, while the cytoplasmic, inactive, fraction was not. A similar pattern of dose-dependent DMF effect was observed for both HO-1 and γGCSc (Fig. 3B) proteins, two antioxidant enzymes which are downstream targets of NRF2, confirming that high concentration of DMF decreases NRF2 activation on the one hand and showcase the functional activation of NRF2 antioxidant pathway by low concentration of DMF on the other. To evaluate the time dependency of this effect, OVCAR3 cells were treated for various times with 100 μmol/L DMF. An early increase in NRF2, HO-1, and γGCSc protein levels were observed between 1 and 8 hours posttreatment. However, from 16 to 24 hours posttreatment, NRF2 protein was abolished, suggesting that DMF has a transient effect on NRF2 induction in OVCAR3 cells (Supplementary Fig. S4B).

To gain an insight into whether high-dose DMF cytotoxicity is dependent on NRF2 inhibition, we used an expression vector to induce NRF2 overexpression in OVCAR3 cells exposed to high concentration of DMF. As shown in Fig. 3C, DMF reduced cell viability, increased intracellular ROS, and depleted intracellular GSH in cells that were transfected with a pGW1 empty vector (EV) alone. NRF2 overexpression, however, prevented DMF-induced cell death, ROS formation, and GSH depletion (Fig. 3C). Furthermore, treating NRF2-overexpressing OVCAR3 cells with the NRF2 small-molecule inhibitor brusatol in combination with 100 μmol/L DMF caused a significant increase in intracellular ROS and cell death compared with either DMF- or brusatol-treated cells alone (Supplementary Fig. S4C and S4D).

Our result shows that GSH depletion, ROS accumulation, and cytotoxicity induced by high-dose DMF are related to NRF2 depletion.

DMF downregulates the NRF2 protein stabilizer DJ-1 in OVCAR3 cells

Chemical structure and previous proteomic data strongly suggest that NRF2 is not a direct target of DMF (32). We therefore hypothesized that DJ-1, which is a "SH"-rich protein known to interact with NRF2 and affect its protein stability and activity (32, 33), could be a target of succination by fumarate. So we first investigated the effect of DMF on DJ-1 in OVCAR3 ovarian cancer cells. As shown in Fig. 3D, a decrease in DJ-1 expression, which correlates with increase in DMF concentration, was observed. Time dependency of this effect was also evaluated and a decrease in DJ-1 expression was observed from 8 hours posttreatment (Supplementary Fig. S4B). A decreased expression of DJ-1 was also observed in a primary lung cancer cell line treated with increasing concentration of DMF (Supplementary Fig. S4E).

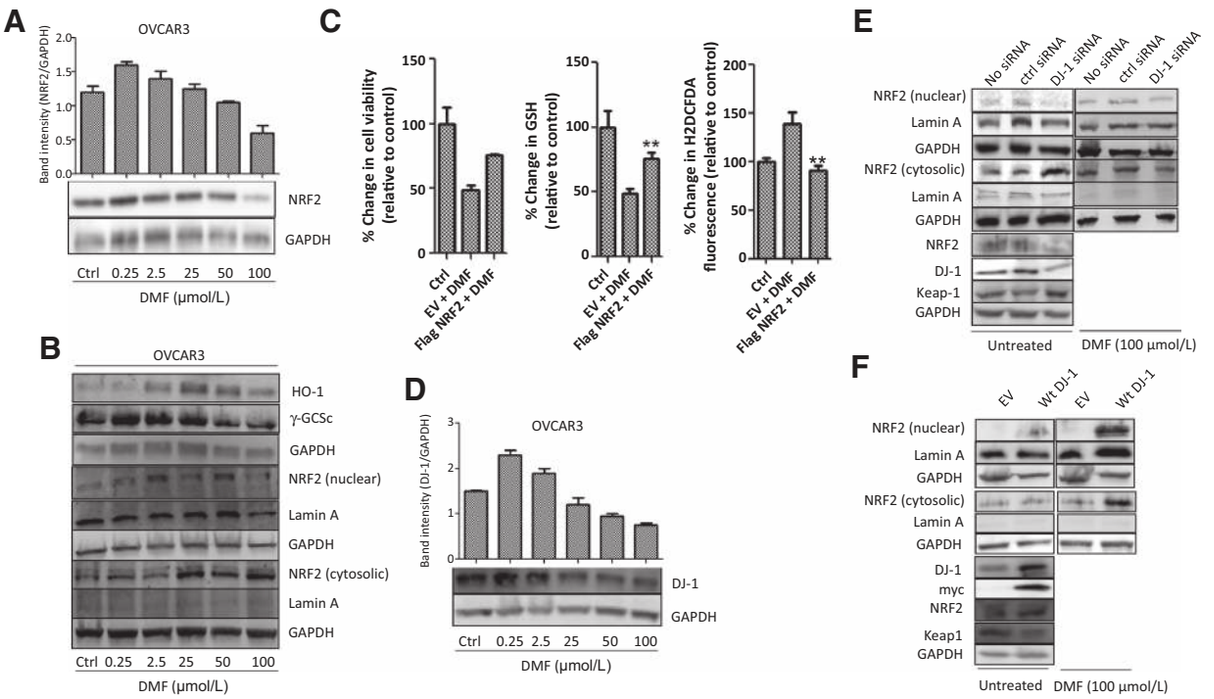

Figure 3.

Modulation of NRF2 expression and activity by DMF in OVCAR3 cells. Cells were either treated with 0.05% DMSO or with increasing concentrations of DMF for 24 hours. Cell lysates were prepared and analyzed on a 10% SDS-polyacrylamide gel followed by Western blottting using an anti- NRF2, HO-1, or γ-GCSc–specific antibody. Relative densitometry for NRF2 is shown in **A**, while the protein levels of HO-1 and γ-GCSc are shown in (**B**, top). Subcellular localization of NRF2 was assessed by immunoblots of nuclear and cytosolic proteins (**B**, bottom). Lamin A was used as a nuclear marker; GAPDH was used as a loading control. One representative of at least two independent Western blots is shown here. **C,** OVCAR3 cells were either left untransfected or transfected, with a control empty vector or the NRF2 plasmid as described in the "Materials and Methods". After transfection, cells were further incubated with or without DMSO and DMF for 24 hours. Cell viability was then determined using the crystal violet assay method (**C**). Cells were also assayed for ROS production and GSH depletion (**C**). Cell lysates from **A** were again analyzed on a 10% SDS-polyacrylamide gel followed by Western blottting using an anti-DJ-1 antibody. Relative densitometry for DJ-1 is shown in **D**. In all the experiments, data are expressed as a percentage change relative to control. In each case, the mean of three independent experiments is shown. *, $P < 0.05$; **, $P < 0.01$. Modulation of cellular effects of high concentrations of DMF by expression level of DJ-1 in OVCAR3 cells. **E** and **F,** OVCAR3 cells were left untransfected (no siRNA) or transfected with nontargeting scramble siRNA (ctrl siRNA), DJ-1 siRNA, wild-type DJ-1 (wt DJ-1), or the control vector pGW1 (EV) with the NIH:OVCAR-3 Cell Avalanche Transfection Reagent. Twenty-four hours after transfection, the cells were left untreated, treated with 0.05% DMSO (ctrl), or with 100 μmol/L DMF for an additional 24 hours. Whole cell, nuclear, and cytosolic lysates were prepared and analyzed on a 10% SDS-polyacrylamide gel followed by Western blottting using the appropriate antibody. **E** and **F,** immunoblots showing the expression of nuclear and cytosolic fractions of NRF2, total NRF2, DJ-1 and KEAP1 in OVCAR3 cells that were left untreated after transfection (left). Right, immunoblots showing the expression of nuclear and cytosolic fractions of NRF2 in OVCAR3 cells that were treated with 100 μmol/L DMF for 24 hours following transfection. Lamin A was used as a nuclear marker, whereas GAPDH was used as a loading control and in each case one representative of at least two independent Western blots is shown.

Expression level of DJ-1 modulates cellular effects of high concentrations of DMF in OVCAR3 cells

To understand the role of DJ-1 in DMF cytotoxicity, expression of DJ-1 was modulated in OVCAR3 cells by DJ-1 siRNA and wild-type DJ-1 expression vector (wt DJ-1). As shown in Fig. 3E, compared with non-siRNA and control siRNA groups, transfection of DJ-1 siRNA in OVCAR3 cells caused not only a decrease in the endogenous protein levels of DJ-1, but also in total and nuclear fractions of NRF2. Lamin A and GAPDH were used as nuclear and cytosolic markers, respectively. Also, compared with the empty vector, overexpression of wt DJ-1 showed an increase in the protein levels of both DJ-1 and NRF2 (Fig. 3F). Similarly, in DMF-treated cells, DJ-1 downregulation induced depletion of nuclear and cytosolic NRF2 fractions, while expression of wt DJ-1 prevented it (Fig. 3E and F). Furthermore, we observed an interaction between NRF2 and DJ-1 (Supplementary Fig. S4F) through immunoprecipitation experiments. These results confirmed the previous observation that DJ-1 favors accumulation of NRF2 and its nuclear translocation. Moreover, DJ-1 level controls NRF2 depletion induced by DMF. We then examined the effect of DJ-1 levels in DMF cytotoxicity.

In cells not treated with DMF, downregulation of DJ-1 did not have any significant effect on cell viability (data not shown) but induced a small amount of apoptosis as evaluated by caspase-3 (Supplementary Fig. S5) and PARP cleavage (Fig. 4A, top left). However, compared with control siRNA–treated cells, downregulation of endogenous DJ-1 made the cells more susceptible to DMF-induced ROS production (Fig. 4B, $P < 0.01$), decreased GSH (Fig. 4B, $P < 0.01$), decreased cell viability (Fig. 4B, $P < 0.01$) and induced apoptosis (Fig. 4A, top right). Overexpression of wt DJ-1 did not modify the amount of caspase-3 (Supplementary Fig. S4A) and PARP (Fig. 4A, bottom left) cleavages in untreated OVCAR3 cells but countered the observed high-dose DMF effect

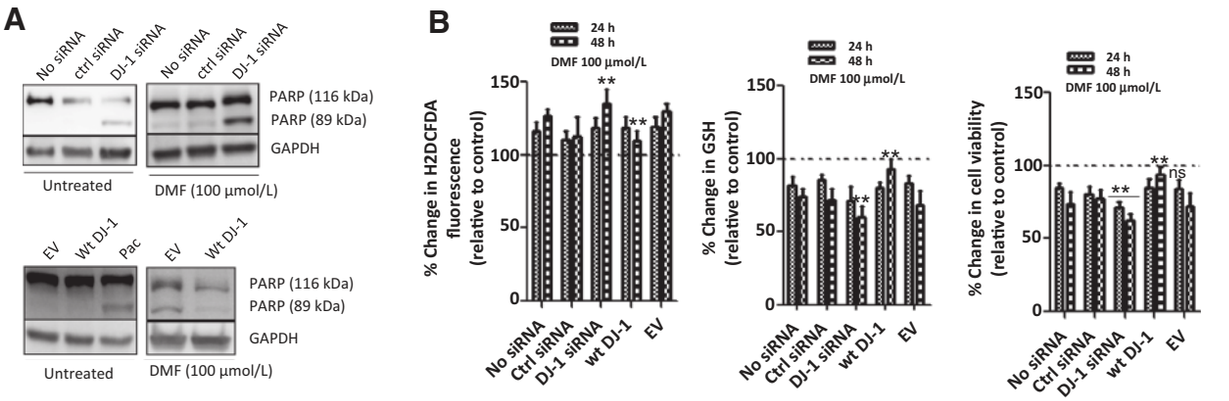

Figure 4.

Modulation of DMF-induced cell death by DJ-1 levels in OVCAR3 cells. **A** and **B,** OVCAR3 cells were left untransfected (no siRNA) or transfected with nontargeting scramble siRNA (ctrl siRNA), DJ-1 siRNA, wild-type DJ-1 (wt DJ-1), or the control vector pGW1 (EV) with the NIH:OVCAR-3 Cell Avalanche Transfection Reagent. Twenty-four hours after transfection, the cells were left untreated, treated with 0.05% DMSO (ctrl), or with 100 µmol/L DMF for an additional 24 and 48 hours. **A,** immunoblots showing PARP cleavage in OVCAR3 cells that were left untransfected (no siRNA) or transfected with nontargeting scramble siRNA (ctrl siRNA) or DJ-1 siRNA (**A**) or transfected with either wt DJ-1 or the empty vector (EV). After transfection, cells were further incubated or not with DMF for 24 hours. GAPDH was used as a loading control and in each case one representative of at least two independent Western blots is shown. Cells were also assayed for ROS, total GSH content and viability (**B**). In all the experiments, data are expressed as a percentage change relative to control. In each case, the mean of three independent experiments is shown. *, $P < 0.05$; **, $P < 0.0$; ns, not statistically significant.

on ROS (Fig. 4B) induction and GSH (Fig. 4B) levels, cell viability (Fig. 4B), and apoptosis (Fig. 4A, bottom right).

DMF has antitumor effects in mice models of colon cancer

To confirm the observations made on cancer cells *in vitro*, the anticancer property of DMF was assessed in two mice models. The preventive effect of DMF was assessed in a first model in which colon cancer was chemically induced in mice by the AOM/DSS combination (Supplementary Fig. S6A; Table 1). After week 20, the incidence of colon cancer in DMF-treated mice appeared lower than in DMSO-treated control mice, as the incidence of rectal prolapses (due to tumor development) was lower and the mean length of the large bowel higher in DMF-treated group (Table 1). Mean body weight was significantly lower in DMSO-treated control mice, compared with DMF-treated mice ($P < 0.05$) and control mice ($P < 0.01$). Nodular, polypoid, or caterpillar-like colonic tumors were macroscopically observed in group 1 and to a lesser extent in group 2, with non in group 3 (Fig. 5A, top; Table 1). These tumors were further histologically diagnosed as tubular adenoma and were more pronounced in DMSO-treated control mice, compared with DMF-treated mice (Fig. 5A, bottom).

As an indirect marker of oxidative stress, the AOPPs concentrations were determined in the serum of control and experimental mice. AOPP levels were significantly increased in DMF-treated mice compared with DMSO control mice, which was in agreement with the *in vitro* data, (Fig. 5B).

In a second model, mice bearing CT26 tumors were treated with DMSO i.p. once daily, "force feeding" DMF once daily, i.p. paclitaxel or a combination of DMF and paclitaxel (Fig. 5C). Mice treated with DMF alone developed smaller tumors than mice treated by DMSO alone from day 9 ($P < 0.05$; Fig. 5C). Paclitaxel was also associated with smaller tumors from day 9 ($P < 0.05$). Tumor sizes were significantly smaller from day 12 in mice treated with DMF + paclitaxel than in mice treated with DMSO ($P < 0.01$), paclitaxel ($P < 0.01$), or DMF ($P < 0.01$) alone. AOPP levels were also significantly increased in DMF- or DMF in combination with paclitaxel-treated mice compared with DMSO control mice (data not shown for CT26 model). To determine the influence of DMF on the NRF2/DJ-1 axis in the CT26 mouse model, Western blot analysis was performed to detect changes in NRF2 and DJ-1 protein expressions, as described in the Materials and Methods section. As shown in Fig. 5C, decreased expression of total NRF2 and DJ-1 were observed in the DMF-treated group compared with the control group. Paclitaxel treatment alone was associated with a slight decrease expression of total NRF2 and DJ-1 compared with control group and combination of paclitaxel and DMF did not induce further decrease. The nuclear, activated, form of NRF2 was further analyzed by IHC in tumors excised from animals in the CT26 mouse model. The percentage of stained nuclei (Fig. 5D; Supplementary Fig. S6A) was significantly lower in mice treated with DMF alone compared with control mice (−14%, respectively; $P < 0.05$) and in mice treated with DMF + paclitaxel

Table 1. The preventive effect of DMF against colon cancer chemically induced in mice by AOP/DSS

Group no.	Cancer induction	Treatment	No. of mice examined	Body weight (g)	Av. length of bowel (mm)	No. of mice with visible prolapses	Av. no. of tumors
1	AOM/DSS	DMSO	9	19.92 ± 1.16	69.72 ± 4.70	4	9 ± 16.86
2	AOM/DSS	DMF, 20 mg/kg	9	21.46 ± 0.89*	80.30 ± 2.10**	1	3 ± 7.50**
3	Non	Drinking water	4	23.67 ± 3.35**	82.99 ± 7.16**	0	0

NOTE: * and ** indicates statistically significant difference from group 1 (*, $P < 0.05$ and **, $P < 0.01$).

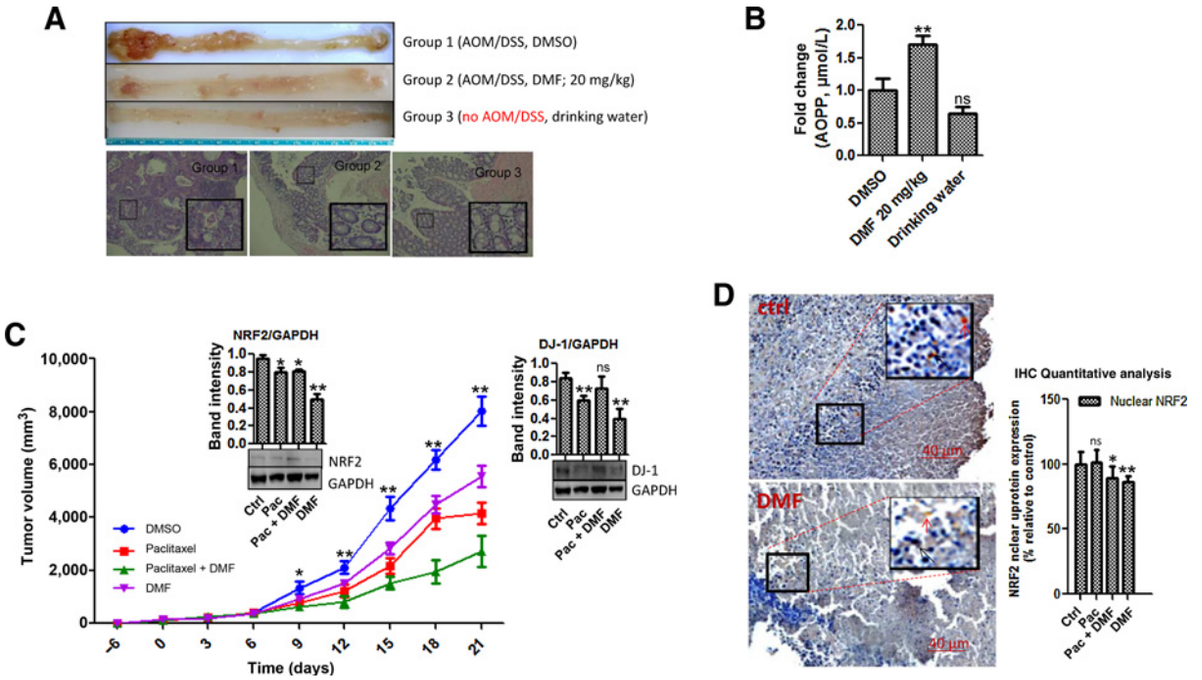

Figure 5.

DMF has antitumor effects *in vivo*. **A,** Macroscopic view of large bowels along with histopathology of colonic neoplasms and and dysplastic lesions of mice in groups 1, 2, and 3. **B,** Bar chart representing mean serum AOPPs in study groups. The chart shows that DMF significantly increases AOPPs in mice. Bars, SEM. **, $P < 0.0$; ns, not statistically significant. **C,** DMF reduces tumor growth in mouse colon carcinogenesis model. Mouse CT26 tumor cells (1.5×10^5) were injected subcutaneously into the back of female BALB/cJRj mice. Treatment was started after clinical appearance of tumors (mean size of 200–500 mm^3, day 0). Mice were treated with DMSO, paclitaxel (Pac), paclitaxel associated with DMF, or DMF alone. Mean values ± SEM of tumor volumes determined from 6 different mice under each condition. Points, mean; bars, SEM. **, $P < 0.01$; *, $P < 0.05$. **C,** Whole-cell lysates from tumor samples were also prepared and analyzed on a 10% SDS-polyacrylamide gel followed by Western blottting using NRF2 or DJ-1 antibodies. GAPDH was used as a loading control. **D,** Representative IHC images of NRF2 expression in mice tumor in different treatment groups along with quantitative analysis of the images. Data are presented as the mean ± SEM; **, $P < 0.01$; *, $P < 0.05$, $n = 6$; blue, nuclei; brown, NRF2; black arrow, localized nuclear NRF2; red arrow, cytosolic NRF2.

compared with mice treated by paclitaxel alone (−12%, respectively; $P < 0.05$).

Taken together, these *in vivo* data show that daily administration of DMF decrease growth of established tumor and prevents tumor formation induced by chronic colic inflammation. Moreover, the observed increase of plasma AOPP, the decrease expression of total and nuclear NRF2 and DJ-1 in CT26 tumors from DMF-treated mice is consistent with the *in vitro* findings regarding modulation of NRF2/DJ-1 axis by DMF.

Discussion

The data presented in this report supports the antitumor effect of DMF and discloses the molecular mechanism model for DMF-induced cancer cell death involving the relative depletion of NRF2 antioxidant system and increased ROS production. DMF is well known for its immunomodulatory effects and has recently been approved for the treatment of psoriasis and relapsing-remitting multiple sclerosis (1–3). It is now also emerging as an anticancer agent as it has been shown to inhibit melanoma (13) and more recently, colon cancer cell growth (12). Nevertheless, the underlying molecular mechanisms involved still remain elusive.

DMF is a methyl-ester of fumarate, an intermediate in the Kreb cycle used by cells to metabolize pyruvate to form ATP. As an endogenous electrophile, fumarate is involved in protein succination, wherein, it spontaneously reacts with cysteine (SH) residues in proteins by a Michael addition reaction to form S-(2-succinyl) cysteine (2SC); and studies have shown that succination of these proteins in cells may impact their functions (32). KEAP1 has been shown to be succinated on two critical cysteine residues by fumarate, which disrupts its interaction with NRF2, resulting in stabilization and accumulation of nuclear NRF2 (ref. 15; Fig. 6). Thus, low concentrations of DMF were reported to exert neuroprotective effects in several noncancer cell models via activation of the NRF2 antioxidant pathway (6, 33). In agreement with these findings, we observed that DMF at lower concentrations (<10 μmol/L) induces nuclear translocation of NRF2 and expression of downstream target genes, *HO-1* and *γGCSc*, in ovarian cancer cells. Moreover, by inducing NRF2, low-dose DMF prevents oxidative stress and cell death induced by paclitaxel

However, our data indicate that at higher concentrations (>25 μmol/L), DMF displays cytotoxicity in several cancer cell lines, induced parallel increase of ROS, elevated levels of oxidized glutathione, and reduced glutathione depletion. Cotreatment with *N*-acetylcysteine demonstrates that DMF cytotoxicity is related to oxidative stress. Surprisingly, such high-dose DMF (>25 μmol/L) was associated with a decrease in total NRF2 protein levels and its nuclear (active) fraction with increasing DMF concentrations, while the (inactive) cytosolic fraction remained unchanged. A similar pattern was observed for both HO-1 and

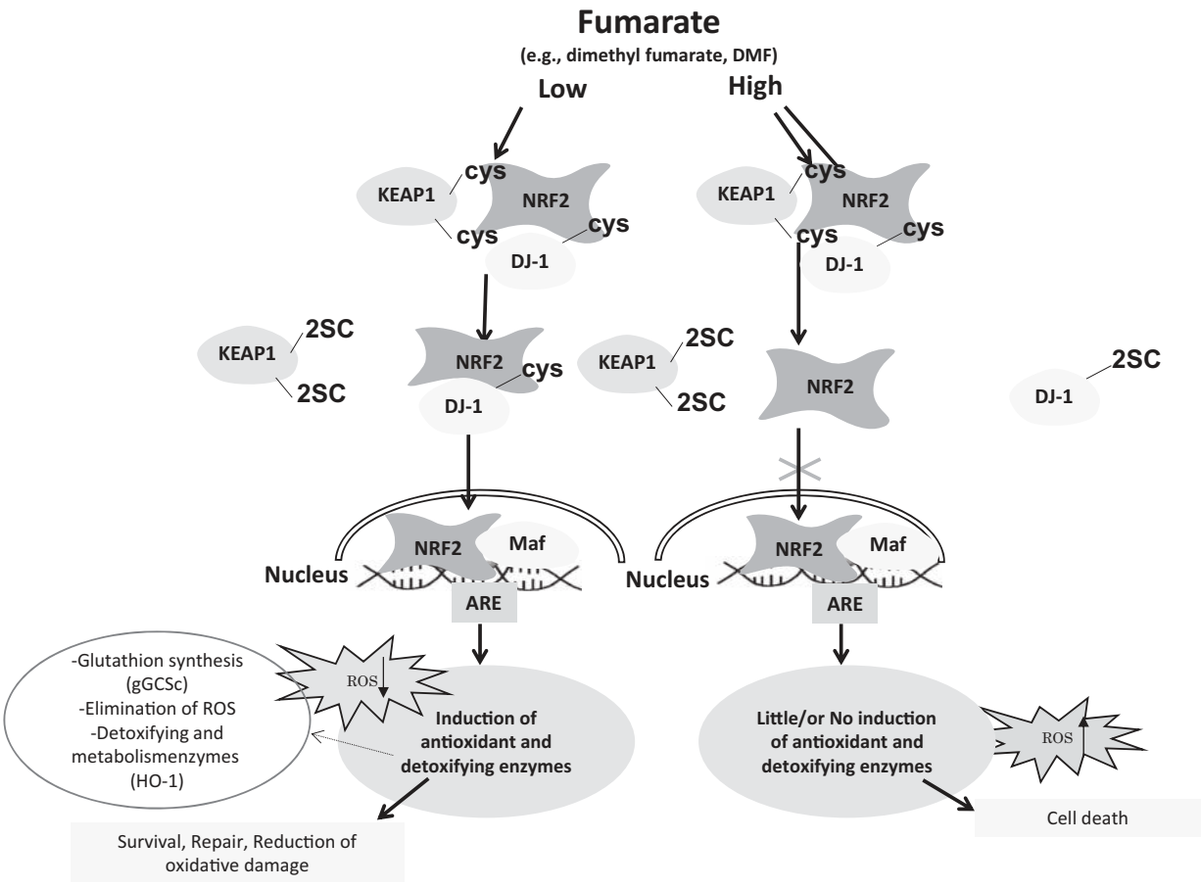

Figure 6.

Proposed mechanism of DMF-induced cancer cell death. Low concentrations of DMF can induce the NRF2 antioxidant pathway, allowing NRF2 nuclear translocation and binding to the antioxidant response elements leading to the transcription of antioxidant and detoxifying enzymes, thereby promoting cell survival. High concentrations of DMF, however, induce disruption of the NRF2 stabilizer DJ-1, which in turn impairs NRF2 induction and transcriptional activities in response to DMF, induces ROS generation, GSH depletion, and hence, facilitates cancer cell death. Cys, cysteine; 2SC, succination of cysteine residues.

γGCSc, confirming the decrease of NRF2 transcriptional activity. The results therefore suggest that at lower concentrations, DMF activates the NRF2 signaling pathway compared with untreated cells, whereas at higher concentrations, this effect disappears and the NRF2 activity tends to be lower than in untreated cells. The transfection of OVCAR3 ovarian cancer cells with the *NRF2* cDNA shows that the observed DMF-induced oxidative stress and cytotoxicity is indeed dependent of NRF2 depletion. Consistent with this finding, results from Western blot analysis and IHC experiments performed in tumor samples from DMF-treated mice showed that the daily administration of 20 mg/kg DMF decreased total NRF2 expression and its nuclear localization. It is likely that the nuclear localization of this pool of NRF2 requires the contribution of other factors such as the NRF2 protein stabilizer DJ-1.

Chemical structure and previous proteomic data (33, 34) strongly suggest that NRF2 is not a direct target of DMF, while the NRF2 protein stabilizer DJ-1 could be. Thus, modifications of its Cys 106 have been associated with a loss of DJ-1 functions and degradation by proteasome (35). Indeed, we observed that high concentration of DMF induced an early concentration-dependent decrease in DJ-1 protein expression in OVCAR3 ovarian cancer cells. DJ-1 has been shown to stabilize the NRF2 protein and increase its nuclear translocation and transcriptional activity by preventing its association with KEAP1 (20). As previously reported (20), we observed by immunoprecipitation experiments a direct interaction between NRF2 and DJ-1. In cancer cells treated with high concentration of DMF, a causal relationship was demonstrated by siRNA and expression vector experiments between decrease DJ-1 protein level in one hand, and nuclear NRF2 depletion, oxidative stress, GSH depletion, and finally cancer cell death, on the other.

These data suggest that not only does high concentration of DMF inhibit KEAP1, but also DJ-1, preventing NRF2 activation (Fig. 6). In this situation, the lethal oxidative stress and glutathione depletion are the result of the impairment of NRF2-mediated antioxidant defense, probably associated with the formation of covalent adducts between fumarate and glutathione, as reported previously (17). NRF2 has long been established as a key molecule for redox homeostasis in cancer cells which produce a large amount of ROS, due to high metabolic activity, mitochondrial dysfunction, or oncogenic activation. DMF could be specifically

active in cancers which develop high NRF2 activity in response to oxidative stress.

We report the antitumoral effects of DMF in two mouse models. In the syngeneic CT26 mouse model, DMF on its own, and to an even greater extent, in combination with paclitaxel, significantly reduces tumor growth. The daily dose of DMF administered to mice was the same as in previous studies of DMF-induced neuro- and cardioprotection (4, 6) but the length of treatment was much shorter in these studies (1–5 days). These observations could be related to DMF tissue accumulation, which is associated with longer treatment or alternatively, to a lesser DMF toxic effect on noncancer cells compared with the malignant ones. This differential effect of DMF may be related to the lower level of oxidative stress in noncancer cells that render the cells more permissive to NRF2 depletion. In addition, previous report showed that activation of the NRF2 antioxidant response pathway is independent of DJ-1 in primary neural cells and tissues, suggesting that the protective role of DJ-1 may be less important for NRF2 function in noncancer cells (36). Even more interesting is the fact that the daily administration of DMF to animals in this CT26 mouse model attenuated the protein levels of both NRF2 and its stabilizer DJ-1, which was yet again consistent with the *in vitro* findings.

In the chemically induced mouse model, DMF prevented weight loss, colon shortening, and rectal prolapse that were associated with colorectal cancer occurrence in DMF-treated animals compared with controls. This clinical effect could in fact be related to inhibition of chronic inflammation induced by DSS (through preventive effect) or to tumor growth inhibition as described in the CT26 model (antitumoral effect). The significant increase of advanced oxidized protein products in the sera of DMF-treated mice indicates that DMF causes oxidative stress in these animals and favors the antitumoral effect hypothesis.

In conclusion, our data support the development of DMF as a new anticancer agent. Its antitumoral effect was observed in two mice models at a dose well-tolerated by humans and applicable to clinical practice (37).The elucidation of the underlying molecular mechanisms involving NRF2–DJ1 interaction may help to identify most sensitive tumors.

Disclosure of Potential Conflicts of Interest

F. Goldwasser is a consultant/advisory board member for Fresenius Kabi. No potential conflicts of interest were disclosed by the other authors.

Authors' Contributions

Conception and design: N.E.B. Saidu, F. Batteux, J. Alexandre
Development of methodology: N.E.B. Saidu, F. Batteux, J. Alexandre
Acquisition of data (provided animals, acquired and managed patients, provided facilities, etc.): N.E.B. Saidu, G. Noé, O. Cerles, L. Cabel, N. Kavian-Tessler, S. Chouzenouxm, C. Chéreau, C. Nicco, B. Borghese, F. Batteux, J. Alexandre
Analysis and interpretation of data (e.g., statistical analysis, biostatistics, computational analysis): N.E.B. Saidu, G. Noé, L. Cabel, N. Kavian-Tessler, S. Chouzenoux, F. Goldwasser, F. Batteux, J. Alexandre
Writing, review, and/or revision of the manuscript: N.E.B. Saidu, O. Cerles, L. Cabel, S. Chouzenoux, K. Leroy, B. Borghese, F. Goldwasser, F. Batteux, J. Alexandre
Administrative, technical, or material support (i.e., reporting or organizing data, constructing databases): N.E.B. Saidu, O. Cerles, S. Chouzenoux, M. Bahuaud, C. Chéreau, F. Batteux, J. Alexandre
Study supervision: N.E.B. Saidu, F. Goldwasser, F. Batteux, J. Alexandre

Grant Support

This work was supported by Comité de Paris de la Ligue contre le Cancer, Martine Midy Foundation, and a Cancer Research for Personalised Medicine (CARPEM) postdoctoral fellowship (to N.E.B. Saidu).

The costs of publication of this article were defrayed in part by the payment of page charges. This article must therefore be hereby marked *advertisement* in accordance with 18 U.S.C. Section 1734 solely to indicate this fact.

Received June 22, 2016; revised December 7, 2016; accepted December 7, 2016; published OnlineFirst January 9, 2017.

References

1. Gold R, Kappos L, Arnold DL, Bar-Or A, Giovannoni G, Selmaj K, et al. Placebo-controlled phase 3 study of oral BG-12 for relapsing multiple sclerosis. N Engl J Med 2012;367:1098–107.
2. Xu Z, Zhang F, Sun F, Gu K, Dong S, He D. Dimethyl fumarate for multiple sclerosis. Cochrane Database Syst Rev 2015;4:CD011076.
3. Papadopoulou A, D'Souza M, Kappos L, Yaldizli O. Dimethyl fumarate for multiple sclerosis. Expert Opin Investig Drugs 2010:19:1603–12.
4. Ashrafian H, Czibik G, Bellahcene M, Aksentijevic D, Smith AC, Mitchell SJ, et al. Fumarate is cardioprotective via activation of the Nrf2 antioxidant pathway. Cell Metab 2013;15:361–71.
5. Pitarokoili K, Ambrosius B, Meyer D, Schrewe L, Gold R. Dimethyl fumarate ameliorates lewis rat experimental autoimmune neuritis and mediates axonal protection. PLoS One 2015;10:e0143416.
6. Scannevin RH, Chollate S, Jung MY, Shackett M, Patel H, Bista P, et al. Fumarates promote cytoprotection of central nervous system cells against oxidative stress via the nuclear factor (erythroid-derived 2)-like 2 pathway. J Pharmacol Exp Ther 2012;341:274–84.
7. Furfaro AL, Traverso N, Domenicotti C, Piras S, Moretta L, Marinari UM, et al. The Nrf2/HO-1 axis in cancer cell growth and chemoresistance. Oxid Med Cell Longev 2016;2016:1958174.
8. Jaramillo MC, Zhang DD. The emerging role of the Nrf2-Keap1 signaling pathway in cancer. Genes Dev 2013;27:2179–91.
9. Konstantinopoulos PA, Spentzos D, Fountzilas E, Francoeur N, Sanisetty S, Grammatikos AP, et al. Keap1 mutations and Nrf2 pathway activation in epithelial ovarian cancer. Cancer Res 2011;71:5081–9.
10. Itoh K, Chiba T, Takahashi S, Ishii T, Igarashi K, Katoh Y, et al. An Nrf2/small Maf heterodimer mediates the induction of phase II detoxifying enzyme genes through antioxidant response elements. Biochem Biophys Res Commun 1997;236:313–22.
11. Itoh K, Tong KI, Yamamoto M. Molecular mechanism activating Nrf2-Keap1 pathway in regulation of adaptive response to electrophiles. Free Radic Biol Med 2004;36:1208–13.
12. Xie X, Zhao Y, Ma CY, Xu XM, Zhang YQ, Wang CG, et al. Dimethyl fumarate induces necroptosis in colon cancer cells through GSH depletion/ROS increase/MAPKs activation pathway. Br J Pharmacol 2015;172:3929–43.
13. Loewe R, Valero T, Kremling S, Pratscher B, Kunstfeld R, Pehamberger H, et al. Dimethylfumarate impairs melanoma growth and metastasis. Cancer Res 2006;66:11888–96.
14. Yamazoe Y, Tsubaki M, Matsuoka H, Satou T, Itoh T, Kusunoki T, et al. Dimethylfumarate inhibits tumor cell invasion and metastasis by suppressing the expression and activities of matrix metalloproteinases in melanoma cells. Cell Biol Int 2009;33:1087–94.
15. Yang M, Soga T, Pollard PJ, Adam J. The emerging role of fumarate as an oncometabolite. Front Oncol 2012;2:85.
16. Chen AF, Kirsner RS. Mechanisms of drug action: The potential of dimethylfumarate for the treatment of neoplasms. J Invest Dermatol 2011; 131:1181.
17. Zheng L, Cardaci S, Jerby L, MacKenzie ED, Sciacovelli M, Johnson TI, et al. Fumarate induces redox-dependent senescence by modifying glutathione metabolism. Nat Commun 2015;6:6001.
18. Lehmann JC, Listopad JJ, Rentzsch CU, Igney FH, von Bonin A, Hennekes HH, et al. Dimethylfumarate induces immunosuppression via glutathione depletion and subsequent induction of heme oxygenase 1. J Invest Dermatol 2007;127:835–45.

19. Malhotra D, Thimmulappa R, Navas-Acien A, Sandford A, Elliott M, Singh A, et al. Decline in NRF2-regulated antioxidants in chronic obstructive pulmonary disease lungs due to loss of its positive regulator, DJ-1. Am J Respir Crit Care Med 2008;178:592–604.
20. Clements CM, McNally RS, Conti BJ, Mak TW, Ting JP. DJ-1, a cancerand Parkinson's disease-associated protein, stabilizes the antioxidant transcriptional master regulator Nrf2. Proc Natl Acad Sci U S A 2006;103:15091–6.
21. De Robertis M, Massi E, Poeta ML, Carotti S, Morini S, Cecchetelli L, et al. The AOM/DSS murine model for the study of colon carcinogenesis: from pathways to diagnosis and therapy studies. J Carcinog 2011;10:9.
22. Tanaka T, Kohno H, Suzuki R, Yamada Y, Sugie S, Mori H. A novel inflammation-related mouse colon carcinogenesis model induced by azoxymethane and dextran sodium sulfate. Cancer Sci 2003;94:965–73.
23. Bissahoyo A, Pearsall RS, Hanlon K, Amann V, Hicks D, Godfrey VL, et al. Azoxymethane is a genetic background-dependent colorectal tumor initiator and promoter in mice: effects of dose, route, and diet. Toxicol Sci 2005;88:340–5.
24. Barderas R, Villar-Vázquez R, Fernandez-Aceñero MJ, Babel I, Paláez-Garcia A, Torres S, et al. Sporadic colon cancer murine models demonstrate the value of autoantibody detection for preclinical cancer diagnosis. Sci Rep 2013;3:2938.
25. Chen H, Li J, Li H, Hu Y, Tevebaugh W, Que J, et al. Transcript profiling identifies dynamic gene expression patterns and an important role for Nrf2/Keap1 pathway in the developing mouse esophagus. PLoS One 2012;7:e36504.
26. Laurent A, Nicco C, Chéreau C, Goulvestre C, Alexandre J, Alves A, et al. Controlling tumor growth by modulating endogenous production of reactive oxygen species. Cancer Res 2005;65:948–56.
27. Alexandre J, Batteux F, Nicco C, Chéreau C, Laurent A, Guillevin L, et al. Accumulation of hydrogen peroxide is an early and crucial step for paclitaxel-induced cancer cell death both *invitro* and *invivo*. Int J Cancer 2006;119:41–8.
28. Strathmann J, Klimo K, Sauer SW, Okun JG, Prehn JH, Gerhauser C, et al. Xanthohumol-induced transient superoxide anion radical formation triggers cancer cells into apoptosis via a mitochondria-mediated mechanism. FASEB J 2010;24:2938–50.
29. Saidu NEB, Abu Asali I, Czepukojc B, Seitz B, Jacob C, Montenarh M. Comparison between the effects of diallyl tetrasulfide on human retina pigment epithelial cells (ARPE-19) and HTC116 cells. Biochim Biophys Acta 2013;1830:5267–76.
30. Saidu NEB, Touma R, Asali IA, Jacob C, Montenarh M. Diallyl tetrasulfane activates both the eIF2α and Nrf2/HO-1 pathways. Biochim Biophys Acta 2013;1830:2214–25.
31. Ren D, Villeneuve NF, Jiang T, Wu T, Lau A, Toppin HA, et al. Brusatol enhances the efficacy of chemotherapy by inhibiting the Nrf2-mediated defense mechanism. Proc Natl Acad Sci U S A 2011: 108:1433–8.
32. Blatnik M, Frizzell N, Thorpe SR, Baynes JW. Inactivation of glyceraldehyde-3-phosphate dehydrogenase by fumarate in diabetes: formation of S-(2-succinyl)cysteine, a novel chemical modification of protein and possible biomarker of mitochondrial stress. Diabetes 2008; 57:41–9.
33. Linker RA, Lee DH, Ryan S, van Dam AM, Conrad R, Bista P, et al. Fumaric acid esters exert neuroprotective effects in neuroinflammation via activation of the Nrf2 antioxidant pathway. Brain 2011;134:678–92.
34. Takaya K, Suzuki T, Motohashi H, Onodera K, Satomi S, Kensler TW, et al. Validation of the multiple sensor mechanism of the Keap1-Nrf2 system. Free Radic Biol Med 2012;53:817–27.
35. Blackinton J, Lakshminarasimhan M, Thomas KJ, Ahmad R, Greggio E, Raza AS, et al. Formation of a stabilized cysteine sulfinic acid is critical for the mitochondrial function of the parkinsonism protein DJ-1. J Biol Chem 2009;284:6476–85.
36. Gan L, Johnson DA, Johnson JA. Keap1–Nrf2 activation in the presence and absence of DJ-1. Eur J Neurosci 2010;31:967–77.
37. Kappos L, Gold R, Miller DH, Macmanus DG, Havrdova E, Limmroth V, et al. Efficacy and safety of oral fumarate in patients with relapsing-remitting multiple sclerosis: a multicentre, randomised, double-blind, placebo-controlled phase IIb study. Lancet 2008;372:1463–72.